6th European Conference on Computational Mechanics (ECCM 6)
7th European Conference on Computational Fluid Dynamics (ECFD 7)
11 – 15 June 2018, Glasgow, UK

A FINITE ELEMENT APPROACH FOR THE ANALYSIS OF VARIABLE CORE DISLOCATIONS

KONSTANTINOS P. BAXEVANAKIS[1] AND ANTONIOS E. GIANNAKOPOULOS[2]

[1]Wolfson School of Mechanical, Electrical and Manufacturing Engineering,
Loughborough University, LE11 3TU, UK
K.Baxevanakis@lboro.ac.uk, http://www.lboro.ac.uk/departments/meme/staff/konstantinos-baxevanakis

[2]Mechanics Division, National Technical University of Athens, Zographou, GR-15773, Greece,
Agiannak@uth.gr, http://www.civ.uth.gr/en/people/professors/37-english/people-bios/653-giannakopoulos-antonios-2

Key words: Dislocation, Disclination, Variable Core, Dislocation Partials.

Abstract. A finite element description of variable core edge dislocations in the context of linear elasticity is presented in this work. The approach followed is based on a thermal analogue and the integral representation of dislocations through stresses. The objective of a variable core defect concept is to eliminate the stress singularity experienced at the dislocation core. This is accomplished assuming that the displacement discontinuity is achieved gradually over some distance. To implement this concept in a finite element scheme, we first model purely rotational crystal defects considering an appropriate pseudo-temperature distribution, which produces a dislocation array of increasing width. Accordingly, we simulate a discrete edge dislocation of linearly increasing width. This description of dislocation core is closer to experimental observations and has a physically anticipated behaviour reproducing the Volterra dislocation away from the core. Further, interactions of variable core dislocations with free boundaries and coupled dislocation partials are investigated. In all cases, we recover the analytical solutions for the stress distributions and the total strain energy.

1 INTRODUCTION

Dislocations are line defects of the crystal lattice with well-documented structure and motion mechanisms. The understanding of dislocation mobility is essential in theories of plasticity, fatigue, and fracture. In the past, several relatively simple geometries have been studied analytically while complex configurations are nowadays tackled through fairly expensive computational schemes. The main reason for this is that the elastic fields of a single Volterra edge dislocation in classical elasticity break down at distances near the dislocation core and lead to r^{-1} singularities [1]. Such stress singularities result in logarithmic singularities for the total strain energy. Therefore, atomistic simulations are often used to model the phenomena near the dislocation core.

In the context of classical linear elasticity, Lubarda and Markenscoff [2] have presented a variable core model (or disclinated dislocation model) that eliminates the stress singularity at the core. This is accomplished assuming that the displacement discontinuity is achieved gradually over some distance that corresponds to the dislocation core. Alternatively, the

variable core dislocation is modelled as a doublet of two wedge disclinations before the limit between them is taken to zero [3]. These rotational crystal defects are also important for the mechanical properties of materials while the disclination concept is convenient for modelling purposes [4, 5].

In the present work we extend our methodology for the implementation of edge dislocations in finite elements [6-8]. As a first-step study, we consider a single wedge disclination lying in an infinite isotropic medium. This defect can be easily incorporated in this framework by selecting a suitable thermal distribution, which produces a dislocation array of increasing width. The derived full field results are in accordance with the theoretical expressions, provided by deWit [9].

Accordingly, we implement the concept of an edge dislocation of variable width. The simplest displacement distribution is a linear increase along the positive *y*-axis. In a more general context any nonlinear increase of the displacement discontinuity may be also interesting. In dislocation theory, this variable displacement discontinuity represents a Somigliana dislocation. Moreover, this core description is closer to experimental observations [10]. Away from the core it has a physically anticipated behaviour reproducing the Volterra dislocation. The produced expression for the dislocation strain energy is bounded and thus can be used as a measure of convergence, which is not the case in the description of Volterra edge dislocations. Then, we study interactions of variable core dislocations in more complex configurations; a variable core dislocation near a free boundary, interaction of coupled dislocation partials in an infinite medium. In all cases, we recover the analytical results of Gars and Markenscoff [11] for the stress distributions and the total strain energy. Other attempts to eliminate dislocation singularities have been reported in the framework of generalized continuum theories [12, 13]. However, it is still unclear how these solutions can be implemented in numerical codes and whether they will be computationally more efficient than the present method.

2 METHODOLOGY

2.1 A discrete wedge disclination in an infinite domain

We consider an elastic solid under plane strain conditions $\left(\varepsilon_{zz}=\varepsilon_{zy}=\varepsilon_{zx}=\sigma_{zy}=\sigma_{zx}=0\right)$. The components of the stress tensor σ_{ij} must obey the equilibrium conditions, which in a Cartesian coordinate system read as

$$\frac{\partial\sigma_{xx}}{\partial x}+\frac{\partial\sigma_{yx}}{\partial y}=0, \quad \frac{\partial\sigma_{xy}}{\partial x}+\frac{\partial\sigma_{yy}}{\partial y}=0, \tag{1}$$

and the components of the linear strain tensor ε_{ij} must meet the local compatibility condition

$$\frac{\partial^2\varepsilon_{yy}}{\partial x^2}-2\frac{\partial^2\varepsilon_{xy}}{\partial x\partial y}+\frac{\partial^2\varepsilon_{xx}}{\partial y^2}=0\,. \tag{2}$$

In a simply connected region, the local compatibility condition (Eq. (2)) is sufficient to ensure continuity and single-valuedness of the displacement field. However, in multiply-connected domains, additional global compatibility conditions must be applied. As discussed by Mindlin

[14] these are expressed in the form of line integrals as

$$\oint d\omega_z = 0, \quad \oint du_x = 0, \quad \oint du_y = 0. \tag{3}$$

where $\omega_z = \frac{1}{2}\left(\frac{\partial u_y}{\partial x} - \frac{\partial u_x}{\partial y}\right)$ is the rotation vector, and $\left(u_x, u_y\right)$ the displacement components. In general, it is not necessary physically that the displacement is single-valued in a multiply-connected region, in which case translational and rotational defects are allowed as follows

$$\oint d\omega_z = \Omega_z, \quad \oint du_x = b_x, \quad \oint du_y = b_y. \tag{4}$$

The first condition in Eq. (4) describes a wedge disclination of Frank vector Ω_z (Fig. 1) while the second and third give the two types of edge dislocations [1].

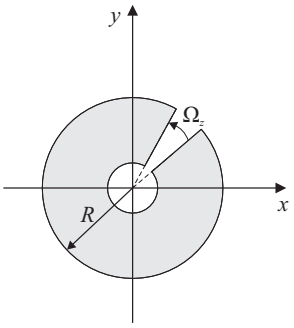

Figure 1: A hollow-core wedge disclination with Frank vector Ω_z.

The conditions of Eq. (4) may be expressed as line integrals on the derivatives of the strain components, or employing the constitutive law, connect the discontinuities with stress components [15].

Following our previous studies on the finite element analysis of dislocations [6-8], we utilize an auxiliary problem of an anisotropic thermoelastic medium with cubic symmetry along the *x* and *y* direction. Considering a thermal distribution $\theta(x, y)$, the constitutive relations between strains and stresses are

$$\begin{aligned} \varepsilon_{xx} &= \frac{1+\nu}{E}\left[\sigma_{xx} - \nu\left(\sigma_{xx} + \sigma_{yy}\right)\right] + \alpha_x(1+\nu)\theta, \qquad \varepsilon_{xy} = \frac{1}{2\mu}\sigma_{xy}, \\ \varepsilon_{yy} &= \frac{1+\nu}{E}\left[\sigma_{yy} - \nu\left(\sigma_{xx} + \sigma_{yy}\right)\right] + \alpha_y(1+\nu)\theta, \end{aligned} \tag{5}$$

where a_x and a_y are the thermal expansion coefficients in the *x* and *y* direction respectively.

Using these constitutive expressions and expressing Michell's conditions (Eq. (4)) in terms of stress components, we introduce a way to produce translational and rotational defects through appropriate thermal distribution schemes. After a few manipulations (see also [7]), Eq. (4) take the form

$$\Omega_z = -(1+\nu)\oint\left(\alpha\frac{\partial\theta}{\partial n}\right)ds,$$
$$b_x = -(1+\nu)\oint\left(\alpha_y y\frac{\partial\theta}{\partial n}-\alpha_x x\frac{\partial\theta}{\partial s}\right)ds,\quad b_y = (1+\nu)\oint\left(\alpha_y y\frac{\partial\theta}{\partial s}+\alpha_x x\frac{\partial\theta}{\partial n}\right)ds, \tag{6}$$

where **n** and **s** are the normal and tangential vectors at any point of a closed contour that surrounds the defects.

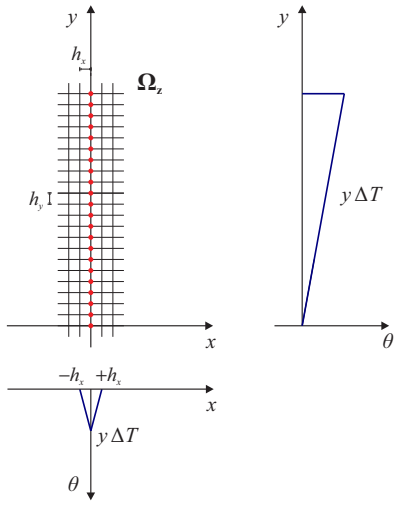

Figure 2: Thermal distribution for the implementation of a wedge disclination to finite elements.

Next, we need to find appropriate thermal distributions to individually create discrete defects. The description of edge dislocations is provided in [7] whereas the plane wedge disclination is modeled as a dislocation array of increasing width. Indeed, the Frank vector is related to the Burgers vector as $b_x = y\,\Omega_z$. To implement this defect, we assume an orthogonal mesh where the element dimensions are h_x and h_y and assign the following distribution on a strip of nodes as shown in Fig. 2

$$\begin{aligned}
&\theta = y\,\Delta T, && x = 0, && y \geq 0,\\
&\theta = y\,\Delta T\frac{x+h_x}{h_x}, && -h_x \leq x \leq 0, && y \geq 0,\\
&\theta = y\,\Delta T\frac{h_x-x}{h_x}, && 0 \leq x \leq h_x, && y \geq 0,\\
&\theta = 0, && \text{everywhere else.}
\end{aligned} \tag{7}$$

This thermal variation produces a wedge disclination as follows

$$\Omega_z = (1+\nu)\alpha_x\,\Delta T\,h_x/y. \tag{8}$$

It is noted that, according to Hirth and Lothe [1], disclinations are not met as discrete defects in

metal crystals since the induced displacement by these defects are unbounded at infinity.

2.2 Variable core edge dislocations

In order to eliminate the stress singularity that arises at the core of discrete edge dislocations, Lubarda and Markenscoff have introduced a variable core edge dislocation [2]. This model assumes that the displacement discontinuity b_x is achieved gradually over some distance ρ (core radius). The defect is essentially produced by the superposition of solutions for two wedge disclinations. A convenient thermal distribution for the implementation of this defect in finite elements is depicted in Fig. 3 and given as [7]

$$\begin{aligned}
&\theta = y\frac{\Delta T}{\rho}, && x = 0, && 0 \le y \le \rho, \\
&\theta = y\frac{\Delta T}{\rho}\frac{x+h_x}{h_x}, && -h_x \le x \le 0, && 0 \le y \le \rho, \\
&\theta = y\frac{\Delta T}{\rho}\frac{h_x-x}{h_x}, && 0 \le x \le h_x, && 0 \le y \le \rho, \\
&\theta = \Delta T, && x = 0, && y \ge \rho, \\
&\theta = \Delta T\frac{x+h_x}{h_x}, && -h_x \le x \le 0, && y \ge \rho, \\
&\theta = \Delta T\frac{h_x-x}{h_x}, && 0 \le x \le h_x, && y \ge \rho, \\
&\theta = 0, && \text{everywhere else.}
\end{aligned} \tag{9}$$

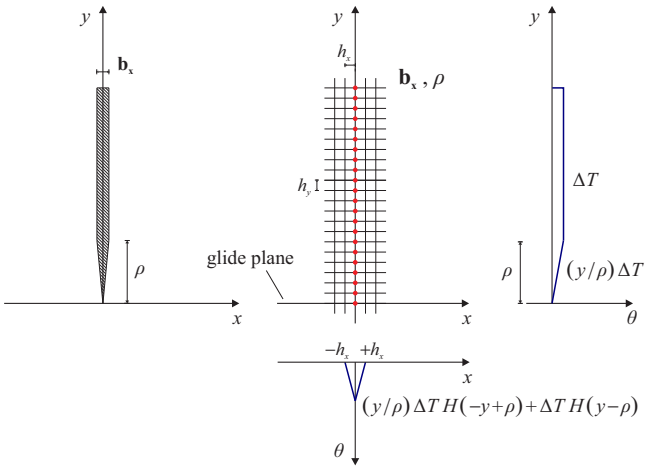

Figure 3: Thermal distribution for the implementation of a variable core edge dislocation into finite elements.

The thermal distribution of Eq. (9) produces a dislocation array of increasing width in the region $0 \le y \le \rho$ for $x = 0$.

3 NUMERICAL EXAMPLES AND DISCUSSION

In this section, we study various configurations where analytical solutions exist in order to examine the accuracy of the proposed methodology.

3.1 Single wedge disclination in an infinite domain

The first geometry studied is that of a discrete wedge disclination in an infinite domain. The defect is considered to lie along the *y*-axis, as described in Fig. 2. In the case of isotropic linear elastic materials, the full-field expressions for the stress components are given as [3, 9]

$$\sigma_{xx} = \frac{\mu\Omega_z}{2\pi(1-\nu)}\left(\ln r + \frac{y^2}{r^2} + \frac{\nu}{1-2\nu}\right), \quad \sigma_{yy} = \frac{\mu\Omega_z}{2\pi(1-\nu)}\left(\ln r + \frac{x^2}{r^2} + \frac{\nu}{1-2\nu}\right),$$
$$\sigma_{xy} = -\frac{\mu\Omega_z xy}{2\pi(1-\nu)r^2}, \quad \sigma_{zz} = \frac{\mu\Omega_z}{2\pi(1-\nu)}\left(2\nu\ln r + \frac{\nu}{1-2\nu}\right), \tag{10}$$

where *r* is the radial distance from the origin and *v* is the Poisson's ratio.

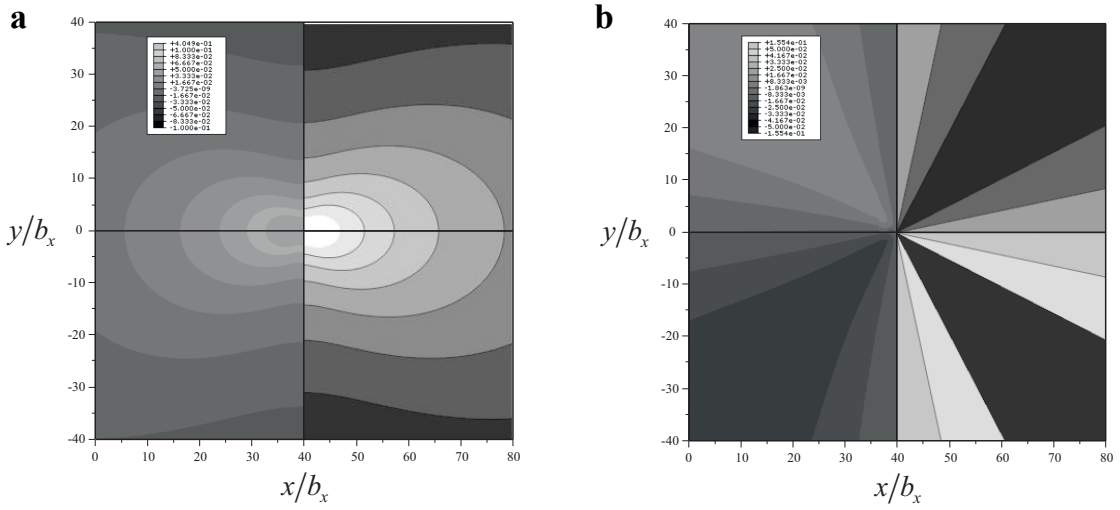

Figure 4: The normalized normal stress fields a) σ_{xx}/b_x and b) σ_{xy}/b_x for a wedge disclination in an infinite isotropic medium. The isocontours range is $(-0.10 \div 0.10)$ Pa/m.

To model this defect a rectangular domain consisting of about 80,000 4-noded quadrilateral plane strain elements was created in ABAQUS [16]. In Table 1, the elastic constants of the material assigned in all problems are provided. It is noted that the thermal expansion coefficients are not the physical ones but take apparent values suitable for computations, since there is no actual temperature field in the problem. In Fig. 4 the numerical results for the normal stress σ_{xx} and the shear stress σ_{xy} are compared to the corresponding analytical solution (Eq. (10)). We observe that the numerical response (left part of each figure) practically coincides with the exact solution near the disclination tip and gradually deviates from it as we move closer to the edge of the analysis domain. The produced response is overall satisfying showing the

robustness of the method.

Table 1: Elastic constants of tungsten [1].

Crystal	c_{11} (10^{10} Pa)	c_{12} (10^{10} Pa)	c_{44} (10^{10} Pa)	H (10^{10} Pa)	A	μ (10^{10} Pa)	E (10^{10} Pa)	ν
W	52.10	20.10	16.00	0.00	1.00	16.00	38.97	0.218

3.2 Discrete edge variable core dislocation in an infinite domain

Next, we examine a variable core edge dislocation lying in an infinite linear elastic isotropic domain. The expression for the shear stress along the x-axis is written as [17]

$$\sigma_{xy}(x,0) = -\frac{\mu b_x}{2\pi(1-\nu)}\frac{x}{x^2+\rho^2}. \tag{11}$$

Accordingly, the total strain energy within a large radius R around the center of the defect is [17]

$$E(R,\rho) = \frac{\mu b_x^2}{4\pi(1-\nu)}\ln\left(\frac{e^{1/2}R}{2\rho}\right). \tag{12}$$

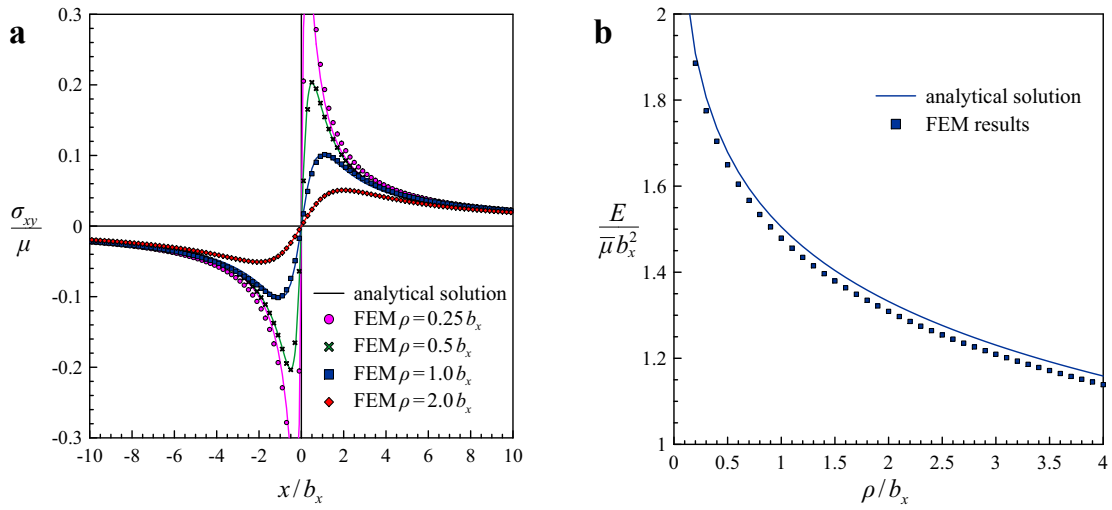

Figure 5: a) Comparison of numerical results with analytical solution for the variation of shear stress σ_{xy} for an edge dislocation of different variable cores. b) Normalized strain energy variation for various core radii ρ.

To study numerically this configuration, we use the same rectangular mesh as before consisting of about 80,000 quadrilateral plane strain elements without any special refinement in the core region. Using a thermal distribution as shown in Fig. 3, we model discrete variable core dislocations of different core radii. The numerical results for the shear stress along the x-axis are compared to the exact solution in Fig. 5a. It is clear that the numerical prediction is in good agreement with the theoretical prediction and the stress field is bounded in all cases. Further, it is observed that as the variable core becomes smaller, the maximum stress is

increased and the overall behaviour approaches that of a Volterra edge dislocation. On the other hand, as the variable core length increases (soft metals), the peak stress reported is lower.

Moreover, the total strain energy for dislocations of various core lengths is plotted in Fig. 5b, where $\bar{\mu} = \mu/2\pi(1-\nu)$. The trend observed in this graph is that the total strain energy is reduced as the variable core length increases. The numerical solution reproduces this response although a constant mismatch from the analytical prediction is noted. In Eq. (12), it is shown that the exact result for the total strain energy depends on the domain of calculation (value of radius *R*). In the finite element implementation of the problem, the contour that surrounds the defect is not a perfect circle since the mesh created is rectangular. Hence, the total strain energy was underestimated by a constant error of ~2%.

3.3 Discrete (single) edge variable core dislocation near a free surface

An extension of the problem studied in the previous section is to consider a variable core dislocation lying at a distance *h* from a free surface, as shown in Fig. 6.

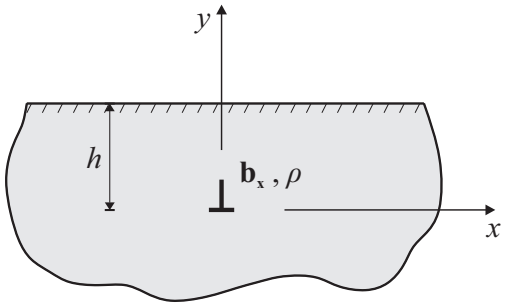

Figure 6: Geometry of a variable core edge dislocation near a free surface.

The shear stress in the glide plane is obtained through superposition of the stress field induced by a variable core dislocation in an infinite domain and a correction field in order to satisfy the boundary conditions at the half-space as follows [11]

$$\sigma_{xy}(x,0) = \sigma_{xy}^{\infty}(x,0) + \sigma_{xy}^{fs}(x,0) =$$

$$= \frac{\bar{\mu} b_x x}{x^2+\rho^2} + \bar{\mu} b_x \left[-\frac{x}{x^2+(\rho+2h)^2} + \frac{4h(\rho+3h)x}{\left(x^2+(\rho+2h)^2\right)^2} - \frac{16h^2(\rho+2h)^2 x}{\left(x^2+(\rho+2h)^2\right)^3} \right]. \tag{13}$$

The total strain energy in this configuration is given as

$$E(h,\rho) = \frac{\bar{\mu} b_x^2}{2} \left[\ln\left(1+\frac{h}{\rho}\right) + \frac{h(h+2\rho)}{2(h+\rho)^2} \right]. \tag{14}$$

We note that Eq. (14) is not dependent on any integration radius *R*.

To analyze numerically this geometry, a mesh of 68,000 quadrilateral plane strain elements was prepared without any refinement near the core or near the free surface. First, defects of

different core widths were placed at a same distance from the free surface, $h = 10b_x$. The results for the stress distribution along the glide plane are reported in Fig. 7a. For the selected distance from the free surface, the results show only a small deviation from the infinite medium case (Fig. 5a). The differences are more noticeable as the defect approaches the free surface $(h \to 0)$ while the infinite medium solution is recovered as $h \to \infty$.

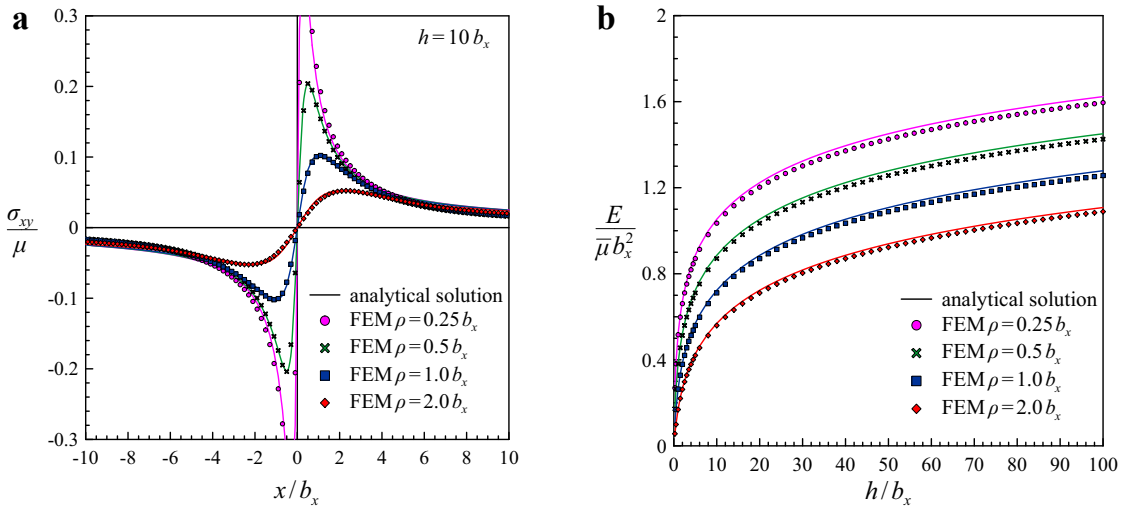

Figure 7: a) Comparison of the shear stress variation predicted by the proposed methodology to the analytical solution for dislocations of different core radii ρ lying at a distance $h = 10b_x$ in tungsten. b) Normalized strain energy variation for different core lengths ρ and distances from the free surface h.

Then, the total strain energy is calculated for four different core lengths and various distances from the free surface (Fig. 7b). Overall, the numerical results match very well with the analytical solution. The total strain energy is minimum when the defect is placed close to the free surface and increases monotonically as the distance h becomes larger approaching asymptotically the corresponding solution for infinite medium as $h \to \infty$ (see Fig. 5b).

3.4 Dissociated edge variable core dislocation in an infinite domain

The last geometry investigated assumes two variable core dislocation partials separated by a distance 2ℓ lying in an isotropic infinite medium (Fig. 8). In general, the two partials may have both edge and screw components, have different Burgers vectors and core radii. The general solution of this problem is provided in [11]. For simplicity, we initially consider two partials having only edge components, with $b_x^{(1)} = b_x^{(2)} = b_x$ and $\rho^{(1)} = \rho^{(2)} = \rho$. In this case, the shear stress along the glide plane is given as

$$\sigma_{xy}(x,0) = \frac{\mu b_x^2}{2\pi(1-\nu)}\left(\frac{x+\ell}{(x+\ell)^2+\rho} + \frac{x-\ell}{(x-\ell)^2+\rho}\right). \tag{15}$$

Also, the total strain energy reads as

$$E = E_s + E_i + E_{sf},$$

$$E_s = \frac{\mu b_x^2}{2\pi(1-\nu)} \ln\left(\frac{e^{1/2} R}{2\rho}\right), \quad E_i = \frac{\mu b_x^2}{2\pi(1-\nu)} \ln\left(\frac{R}{\sqrt{4\ell^2 + \left(\rho^{(1)} + \rho^{(2)}\right)^2}}\right), \quad E_{sf} = 2\gamma\ell, \tag{16}$$

where E_s is the energy of a single dislocation, E_i is the interaction energy of the two partials, and E_{sf} is the stacking fault energy where $\gamma = 500\, mJ\, m^{-2}$ for tungsten [18]. We note that the total strain energy is dependent on an integration radius *R*.

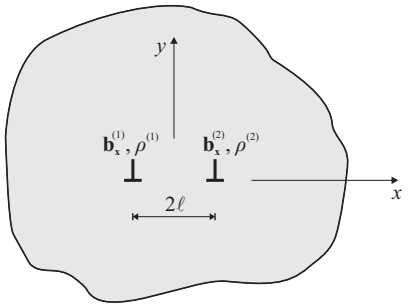

Figure 8: A dissociated variable core edge dislocation in an isotropic infinite medium.

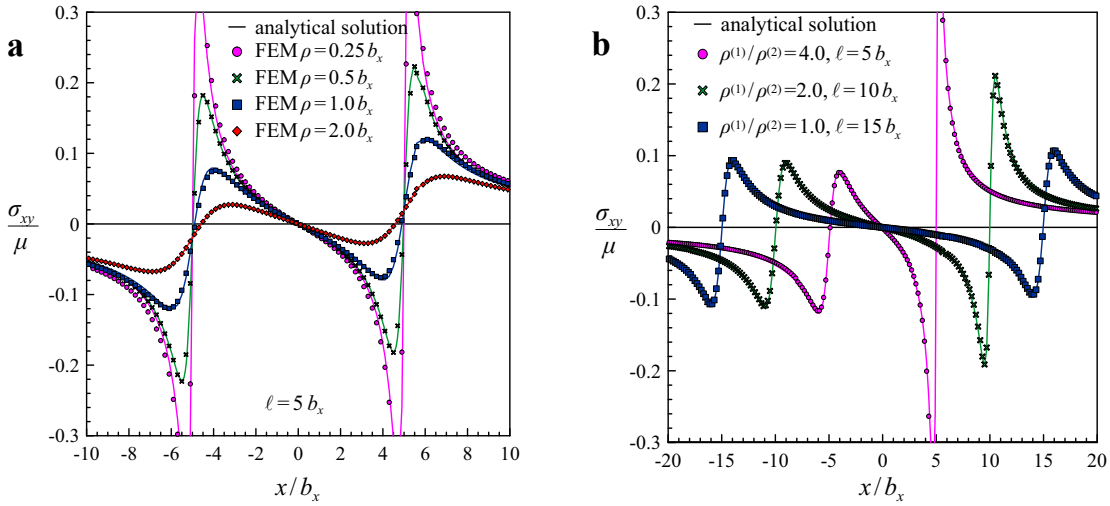

Figure 9: a) Shear stress distributions σ_{xy} for a) various core radii $(\rho_1 = \rho_2)$ and a dissociation distance $2\ell = 10 b_x$, b) various core ratios $\left(\rho^{(1)}/\rho^{(2)}\right)$ and dissociation distance 2ℓ.

For the implementation of this geometry to finite elements, a rectangular mesh of 80,000 quadrilateral plane strain elements is used. Both defects are implemented based on the thermal distribution of Eq. (9) and Fig. 3. In Fig. 9, the shear stress distribution along the glide plane is given for dislocations of various core radii and a constant dissociation distance $\ell = 5 b_x$. It is

observed that the maximum shear stress diminishes as the core radius is increased. In addition, we investigate the problem for dislocation partials that have different core lengths $\left(\rho^{(1)} \neq \rho^{(2)}\right)$ and various dissociations distances. In this case, the analytical expression is obtained through superposition of Eq. (15) for the two defects. The results of this investigation are given in Fig. 9b. It is shown that as the dissociation distance decreases, the maximum shear stress increases, when the core radii are kept constant. As $\ell \to 0$, the response obtained is that of a single variable core dislocation in infinite medium (Fig. 5a). In all cases, the exact solution is very well recovered from the numerical method.

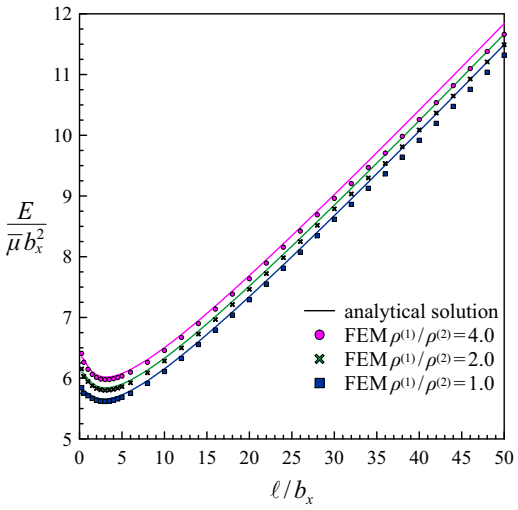

Figure 10: Normalized strain energy variation for different core ratios $\rho^{(1)}/\rho^{(2)}$ and dissociation distance 2ℓ.

Further, the total strain energy was calculated for the same pair of different core partials and various dissociation distances (Fig. 10). We observe that the total strain energy decreases as the dissociation distance increases until a bounded minimum is reached for $\ell/b_x = 3$. Then, the stacking fault energy term becomes dominant over the other two terms of Eq. (16) so that the total strain energy monotonically increases as the dissociation distance of the partials becomes larger. Also, the response is augmented as the core radii ratio $\rho^{(1)}/\rho^{(2)}$ increases.

4 CONCLUDING REMARKS

In this study a finite element approach to analyze disclinations and variable core dislocations was presented. The approach followed is based on the implementation of a thermoelastic problem. The applications investigated were restricted to isotropic cases as the objective was to benchmark the method against known analytical solutions. However, the scheme can be readily extended to study anisotropic crystals.

In all cases, the elastic fields produced by the finite element method were in good accordance with the theoretical expressions of and the maximum stress values are verified. The results of this work are expected to be useful in the analysis of plastic yield strength, giving quantitative results regarding the influence of thin film constraints and dislocation partials interaction.

REFERENCES

[1] Hirth, J.P. and J. Lothe. *Theory of dislocations (2nd Ed.)*. Wiley, New York, (1982).

[2] Lubarda, V. and X. Markenscoff. Configurational force on a lattice dislocation and the Peierls stress. *Arch. Appl. Mech.* (2007) **77**: 147-154.

[3] Eshelby, J.D. A simple derivation of the elastic field of an edge dislocation. *Brit. J. Appl. Phys.* (1966) **17**: 1131.

[4] Romanov, A.E. Mechanics and physics of disclinations in solids. *Eur. J. Mech. A-Solid.* (2003) **22**: 727-741.

[5] Romanov, A.E. and V.I. Vladimirov. Disclinations in solids. *Phys. Status Solidi A* (1983) **78**: 11-34.

[6] Baxevanakis, K.P. and A.E. Giannakopoulos. Finite element analysis of discrete circular dislocations. *Comput. Model. Eng. Sci.* (2010) **60**: 181-198.

[7] Baxevanakis, K.P. and A.E. Giannakopoulos. Finite element analysis of discrete edge dislocations: Configurational forces and conserved integrals. *International Journal of Solids and Structures* (2015) **62**: 52-65.

[8] Giannakopoulos, A.E., K.P. Baxevanakis, and A. Gouldstone. Finite element analysis of Volterra dislocations in anisotropic crystals: A thermal analogue. *Arch. Appl. Mech.* (2007) **77**: 113-122.

[9] deWit, R. Theory of disclinations: IV. Straight disclinations. *J. Res. Natl Bureau Standards Sect. A, Phys. Chem. A* (1973) **77**: 607-658.

[10] Vitek, V. Structure of dislocation cores in metallic materials and its impact on their plastic behaviour. *Prog. Mater. Sci.* (1992) **36**: 1-27.

[11] Gars, B. and X. Markenscoff. The Peierls stress for coupled dislocation partials near a free surface. *Philos. Mag.* (2012) **92**: 1390-1421.

[12] Gutkin, M.Y. and E.C. Aifantis. Dislocations and Disclinations in Gradient Elasticity. *Phys. Status Solidi B* (1999) **214**: 245-284.

[13] Lazar, M. and G.A. Maugin. Nonsingular stress and strain fields of dislocations and disclinations in first strain gradient elasticity. *Int. J. Eng. Sci.* (2005) **43**: 1157-1184.

[14] Mindlin, R.D. and M.G. Salvadori. *Analogies*, in: M. Hetenyi (Ed.), *Handbook of Experimental Stress Analysis*. John Wiley & Sons, New York, (1950).

[15] Dundurs, J. and X. Markenscoff. Invariance of stresses under a change in elastic compliances. *Proc. R. Soc. Lond. A* (1993) **443**: 289-300.

[16] ABAQUS. version 6.13, 2013. User's Manual. Dassault Systems, Pawtucket, RI., (2013).

[17] Lubarda, V.A. and X. Markenscoff. Variable core model and the Peierls stress for the mixed (screw-edge) dislocation. *Appl. Phys. Lett.* (2006) **89**: 151923-3.

[18] Hartley, C. On the dissociation of dislocations on {112} planes of anisotropic bcc metals. *Acta Metallurgica* (1966) **14**: 1133-1136.